Rational approximation of rotation minimizing frames using Pythagorean–hodograph cubics

Christoph Mäurer, Bert Jüttler

Fachbereich Mathematik, Technische Universität Darmstadt
Schloßgartenstraße 7, 64289 Darmstadt, Germany
emails: fa-twt-christoph.maeurer@daimlerchrysler.com,   juettler@mathematik.tu-darmstadt.de

Abstract.   This article is devoted to the rotation minimizing frames that are associated with spatial curves. Firstly we summarize some results concerning the differential geometry of the sweeping surfaces which are generated by these frames (the so–called profile or moulding surfaces). In the second part of the article we describe a rational approximation scheme. This scheme is based on the use of spatial Pythagorean hodograph (PH) cubics (also called cubic helices) as spine curves. We discuss the existence of solutions and the approximation order of G^1 Hermite interpolation with PH cubics. It is shown that any spatial curve can approximately be converted into cubic PH spline form. By composing the rational Frenet–Serret frame of these curves with suitable rotations around the tangent we develop a highly accurate rational approximation of the rotation minimizing frame. This leads to an approximate rational representation of profile surfaces.

Keywords: Rotation minimizing frame, Pythagorean–hodograph curves, sweeping surface, profile surface, moulding surface.
MSC 1994: 53A04, 68U05.

1. Introduction

Many techniques of computer–aided surface design are based on *moving frames* associated with a (planar or spatial) *spine curve*. This includes sweeping and lofting techniques, but also rolling ball blends. For instance, a so–called *sweeping surface* is obtained from the parametric representation

$$\mathsf{s}(u,v) = \mathsf{x}(v) + A(v)\,\mathsf{c}(u) = \mathsf{x}(v) + c_2(u)\,\vec{\mathsf{f}}_2(v) + c_3(u)\,\vec{\mathsf{f}}_3(v), \tag{1}$$

where $\mathsf{x}(v)$ is the (at least G^1-continuous) spine curve with parameter $v \in [v_0, v_1] \subset \mathbb{R}$. Here, the planar cross–section (or profile) curve is given by the parametric representation

$\mathsf{c}(u) = (0, c_2(u), c_3(u))^\top$ with another parameter $u \in [u_0, u_1] \in \mathbb{R}$. The special orthogonal matrix

$$A(v) = \{\vec{\mathsf{t}}(v), \vec{\mathsf{f}}_2(v), \vec{\mathsf{f}}_3(v)\} \tag{2}$$

specifies the moving frame. The moving frame is defined by the tangent vector $\vec{\mathsf{t}}(v) = \dot{\mathsf{x}}(v)/\|\dot{\mathsf{x}}(v)\|$ of the spine curve, along with unit vectors $\vec{\mathsf{f}}_2(v), \vec{\mathsf{f}}_3(v)$ spanning the normal plane of the spine curve at $\mathsf{x}(v)$. The sweeping surface $\mathsf{s}(u, v)$ is generated by moving the cross section curve $\mathsf{c}(u)$ along the spine curve $\mathsf{x}(v)$ with the orientation as specified by $A(v)$. A remarkable illustration of a sweeping surface has been given by Bézier in Figure 12 of his preface to Farin's textbook [2].

Clearly, sweeping surfaces can easily be generalized by allowing the profile curve to evolve during the motion, or by using non–orthogonal matrices $A(v)$, cf. e.g. [19]. This leads to the so–called 'generalized cylinder' surfaces that are frequently being used in Computer Animation and Geometric Modeling [10].

In this paper, however, we confine ourselves to rigid profile curves and special orthogonal matrices $A(v)$. The results may also serve as a starting point for the design of more general surfaces, by adding additional transformations.

The present paper is devoted to two problems that are related to the design of the moving frame $A(v)$ and the associated sweeping surface $\mathsf{s}(u, v)$.

- *Shape.* After choosing both the spine and the profile curves, the sweeping technique leaves the designer with one degree of freedom, as it is still possible to rotate the frame $A(v) = \{\vec{\mathsf{t}}(v), \vec{\mathsf{f}}_2(v), \vec{\mathsf{f}}_3(v)\}$ around the tangent $\vec{\mathsf{t}}$. Clearly, the choice of this rotation has a strong influence on the shape of the resulting sweeping surface.

- *Rational representations.* The piecewise polynomial and rational parametric representations have gained a paramount position as descriptions for curves and surfaces. However, a sweeping surface which is generated by a rational spine curve and a rational cross section curve is generally not rational. This is due to the fact, that not every rational space curve also has an associated rational frame. In order to apply the Bézier or B-spline technique to the moving frame, it is desirable that the corresponding moving frame is rational, too.

The shape problem will be handled with the help of the so–called *rotation minimizing frames* (RMF) that are associated with spatial curves. In Computer Aided Geometric Design, these frames have firstly been studied by Klok [11]. Among the possible frames of a given spine curve, they exhibit the minimum intrinsic rotation around the tangent vector of the curve. Consequently, in comparison with other frames (such as the well–known Frenet–Serret frame (FSF) of a spine curve, see [19]), using the rotation minimizing frame of a spine curve has several advantages. In particular it can be observed that the sweeping surfaces generated by the RMF exhibit better shapes than other sweeping surfaces in general. This fact is illustrated by Fig. 1, showing sweeping surfaces which are generated by the rotation minimizing frame (left) and by the Frenet–Serret frame (right) of a given spine curve (thick line). In addition to the surfaces, the normal planes of the spine curve at the segment end points have been drawn.

More precisely, the RMF–generated sweeping surfaces enjoy a number of remarkable differential geometric properties. The second part of the paper discusses these properties in somewhat more detail.

In order to address the problem of finding a rational representation, we will use spatial *Pythagorean Hodograph* (PH) curves as spine curves. These curves have been introduced by
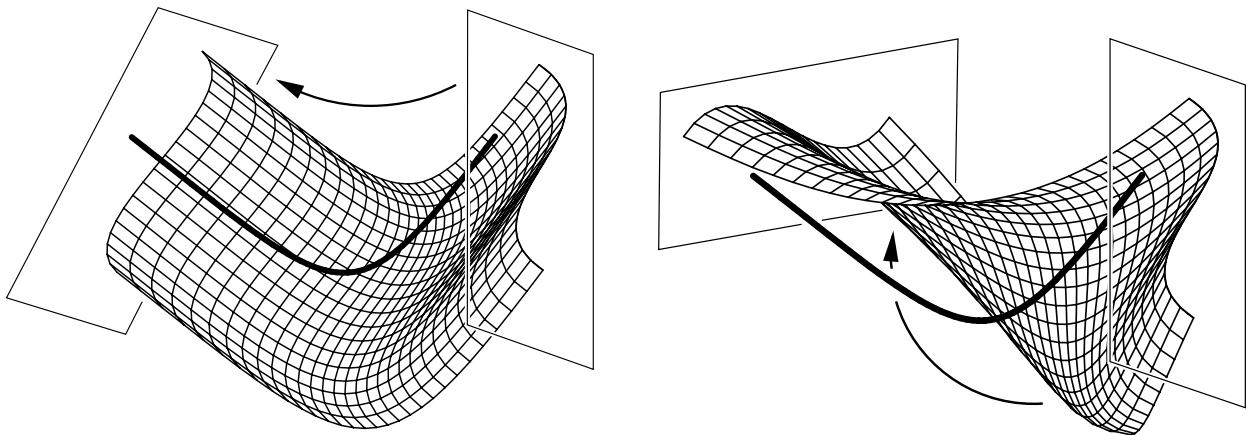
Figure 1: Sweeping surfaces generated by the rotation minimizing frame (left) and
by the Frenet–Serret frame.

Farouki and Sakkalis [3]. In our application, these curves are identified as the rational curves
which possess an associated rational frame $A(v)$.

As proposed by Pottmann and Wagner [15, 16], RMF–generated sweeping surface will be
called *profile surfaces*. Unfortunately, profile surfaces with rational spine curve and rational
cross section are generally not rational, even if the spine curve is a Pythagorean hodograph
curve. Recently, Pottmann and Wagner [15] have presented a method for constructing rational
profile surfaces. Their approach is based on the so–called dual representations, where a surface
is considered as the envelope of its tangent planes. This method, however, leads to relatively
high polynomial degrees which may be disadvantageous in applications.

In Section 3 we propose another approach, as follows. We derive a technique for computing
a rational representation of sweeping surfaces with the help of piecewise cubic Pythagorean
hodograph (PH) spine curves. Then, in a second step, this class of surfaces is used for
approximating the profile surface.

Spatial cubic PH curves form a remarkable class of curves, see Section 3 for details.
In particular, these curves can be used for G^1 Hermite interpolation (i.e. interpolation of
boundary points with associated unit tangents). With the help of certain properties of the
control polygon which were revealed by Farouki and Sakkalis [3], Wagner and Ravani [19] have
developed a G^1–Hermite interpolation scheme with spatial PH cubics. A slightly different ap-
proach, along with a detailed analysis of the existence and the behaviour of the solutions, has
been presented earlier by the authors [6, 8]. Either technique can be used for approximately
converting a given spatial spine curve into cubic PH form, with any desired accuracy. As
shown in the recent Master thesis of Eriksson [1], the approximation order of G^1 Hermite
interpolation with spatial PH cubics is four. This observation generalizes a similar result for
planar PH cubics [14].

In Section 3 of this paper we derive an exact representation of the rotation minimizing
frames that are associated with spatial PH cubics, involving trigonometric functions. Then
we present a numerical optimization technique to compute a *rational* approximation to the
RMF. The results are illustrated by several examples.

2. Rotation minimizing frames and profile surfaces

This section is devoted to the so–called *profile surfaces*. These surfaces are the sweeping surfaces generated via equation (1) by the rotation minimizing frame (RMF), cf. [16]. From a slightly different point of view, they have been studied as *moulding surfaces* (in the German literature: 'Gesimsflächen') in classical differential geometry, cf. [17]. This section aims to summarize some of the classical results and the connection with the more recent ones [16]. In addition we study certain properties of profile surfaces which are particularly important in surface design, such as continuity, differentiability, curvature distribution, convexity and offsets.

2.1. Rotation minimizing frames

Recall that the Frenet–Serret frame $\{\vec{t}, \vec{n}, \vec{b}\}$ of a given space curve $\mathsf{x}(v)$ is formed by the tangent, normal, and binormal vectors of the curve,

$$\vec{t}(v) = \frac{\dot{\mathsf{x}}(v)}{\|\dot{\mathsf{x}}(v)\|}, \quad \vec{b}(v) = \frac{\mathsf{k}^{(r)}(v)}{\|\mathsf{k}^{(r)}(v)\|}, \quad \vec{n}(v) = \vec{b}(v) \times \vec{t}(v), \tag{3}$$

with

$$\mathsf{k}^{(r)}(v) = \dot{\mathsf{x}}(v) \times \mathsf{x}^{(r)}(v), \tag{4}$$

where $r \geq 2$ is the order of the first derivative that is linearly independent of $\dot{\mathsf{x}}(v)$. The given curve is assumed not to be a straight line. In addition, we assume that the curve is regular, hence $\dot{\mathsf{x}}(v) \neq \vec{0}$.

The Frenet–Serret frame is the standard tool for studying the differential geometry of spatial curves. For applications in geometric modeling, however, the Frenet–Serret frame is not the best choice, since it may exhibit a strong rotation around the tangent vector of the spine curve. In order to avoid this disadvantage, the so–called *rotation minimizing frame* (RMF) has been studied in the literature, see e.g. [4, 7, 11, 15, 16, 20]. The rotation minimizing frame (2) is characterized by the fact that the vectors $\vec{f}_2(v)$ and $\vec{f}_3(v)$ (which span the normal plane) rotate as little as possible around the tangent vector $\vec{t}(v)$. The different behaviour of both frames has already been visualized in Fig. 1.

In relation to the Frenet–Serret frame, the RMF can be represented as

$$\begin{aligned}
\vec{f}_2(v) &= \sin \Omega(v)\, \vec{b}(v) + \cos \Omega(v)\, \vec{n}(v), \\
\vec{f}_3(v) &= \cos \Omega(v)\, \vec{b}(v) - \sin \Omega(v)\, \vec{n}(v).
\end{aligned} \tag{5}$$

with a certain angle $\Omega(v)$. The angle Ω specifies the difference of the two frames; it can be computed from the integral formula

$$\Omega(v) - \Omega_0 = - \int_{v_0}^{v} \tau(t)\, \|\dot{\mathsf{x}}(t)\|\, dt \tag{6}$$

with the integration constant Ω_0, see [4]. Here, $\tau = \det\{\dot{\mathsf{x}}, \ddot{\mathsf{x}}, \dddot{\mathsf{x}}\}/\|\dot{\mathsf{x}} \times \ddot{\mathsf{x}}\|^2$ is the *torsion* of the spine curve. Consequently, the Frenet–Serret frame and the RMF coincide if and only if the spine curve $\mathsf{x}(v)$ is planar, i.e. $\tau \equiv 0$.

In order to justify the name *rotation minimizing* frame, we compute the derivatives of the frame vectors $\vec{f}_i$:

$$\begin{aligned}
\frac{d}{dv}\vec{f}_2 &= -\kappa\cos\Omega\,\dot{x} + \left(\tau\|\dot{x}\| + \dot{\Omega}\right)\left(\cos\Omega\,\vec{b} - \sin\Omega\,\vec{n}\right), \\
\frac{d}{dv}\vec{f}_3 &= \kappa\sin\Omega\,\dot{x} - \left(\tau\|\dot{x}\| + \dot{\Omega}\right)\left(\sin\Omega\,\vec{b} + \cos\Omega\,\vec{n}\right),
\end{aligned} \tag{7}$$

where $\kappa(v) = \|\dot{x}\times\ddot{x}\|/\|\dot{x}\|^3$ is the curvature of $x(u)$. In consequence of (6), both the coefficients of the normal and of the binormal vector vanish, hence we have:

Proposition 1 *Consider a point* p *in the normal plane of the spine curve* $x(v)$. *The tangent vector of its trajectory* $x(v) + A(v)p$ *that is generated by the rotation minimizing frame is always parallel to the tangent vector of the spine curve.*

That is, the RMF is the unique frame without intrinsic rotation around the tangent vector of the spine curve.

Remark. For general space curves, using the Frenet frame may lead to difficulties, as it may behave badly at points with vanishing curvature. Consequently, expressing the RMF with respect to the Frenet frame may entail numerical problems. However, we are mainly interested in the RMF of PH cubics. As an advantage, these curves have an associated rational Frenet frame. Note that PH cubics can have points with vanishing curvature only if they are degenerated into straight lines. Consequently, the Frenet frame of general PH cubics is well defined everywhere. Moreover, it is possible to derive an explicit representation of the RMF using elementary functions.

2.2. Profile surfaces

First we analyze the case, that the cross–section curve $c(u)$ is degenerated into a straight line, thus generating a *ruled profile surface*. According to Proposition 1, all tangent vectors $(\partial/\partial v)\,s(u,v)$ of the ruled profile surface for fixed v are parallel to $\dot{x}(v)$, hence

Proposition 2 *If the cross–section curve is a straight line, then the profile surface is a developable surface.*

The generators of a developable are the lines of curvature of the surface. Since the parameter lines of the profile surface form a orthogonal net, we obtain from (1) a parameterization by curvature lines. This property holds for arbitrary cross–section curves.

Proposition 3 *The isoparametric curves* $u = const.$ *or* $v = const.$ *of a profile surface* $s(u,v)$ *are the lines of curvature.*

Proof: We will use the classical Theorem of Joachimsthal [18, Exercise 3, p. 103], which states that any two of the following properties,

    (*i*) the surfaces S_1 and S_2 intersect along a curve C at a constant angle φ,

    (*ii*) the curve C is curvature line on S_1, and

    (*iii*) the curve C is a line of curvature on S_2,

imply the third one. Two profile surfaces which share their spine curves intersect at a constant angle φ. This angle is simply the angle at the intersection of the cross–section curves. Let S_1 be a developable profile surface (generated by a straight line) and S_2 a profile surface with same spine curve but an arbitrary cross–section curve. Joachimsthal's theorem gives the desired result.   □

Surface patches whose parameter lines are lines of curvature have been introduced in geometric design applications by Martin [13] as the so–called *principal patches*, see also [15]. As a remarkable representative, this class of surfaces includes Dupin cyclides.

   In several applications (such as NC-milling or layered manufacturing) one has to compute the *offset* $s_d(u,v) = s(u,v) + d\,\vec{N}(u,v)$ of a given surface $s(u,v)$ at a certain distance d. In the case of profile surfaces, the surface normal $\vec{N}(u,v)$ is contained in the normal plane of the spine curve $x(v)$, because it is perpendicular to $(\partial/\partial v)s(u,v)$. Consequently, surface normal and normal of the cross–section curve are identical.

Proposition 4 *Consider a profile surface* $s(u,v)$ *with spine curve* $x(v)$ *and cross–section curve* $c(u)$. *Let* $c_d(u)$ *be the the (planar) offset of the cross–section at distance* d. *Then the offset* $s_d(u,v)$ *of the profile surface* $s(u,v)$ *is again a profile surface, generated by the spine curve* $x(v)$ *and cross–section curve* $c_d(u)$.

That is, the offsetting operation for profile surface can be reduced to the offsetting of planar profile curves, which is much easier to deal with.

   Next we analyze the relation between the continuity and differentiability of the spine curve and of the corresponding profile surface. For instance, consider a sweeping surface that is generated by a frame associated with a C^2 spine curve (e.g., a cubic B-spline curve). If the Frenet–Serret frame (3) is used, then the resulting surface is generally only continuous, but not G^1. Using profile surfaces and rotation minimizing frames, by contrast, it is possible to avoid this disadvantage:

Proposition 5 *A profile surface with* G^1–*continuous spine and cross–section curves is* G^1–*continuous, too.*

Proof: The tangent plane of a profile surface is spanned by the derivatives $(\partial/\partial u)\,s(u,v)$ (tangent vector of the cross–section curve) and $(\partial/\partial v)\,s(u,v)$. Due to Proposition 1, G^1-continuity of the spine curve implies continuity of the derivative $(\partial/\partial v)\,s(u,v)$, hence tangent plane continuity.   □

In order to analyze higher continuity of profile surfaces we appeal to a classical result on profile surfaces, see [15, 16, 17]. The profile surface can be generated by a motion, as follows. Consider the cross–section curve as a fixed curve in the normal plane of the spine curve. If the normal plane rolls without gliding on an auxiliary developable surface Φ, then the cross–section curve generates the profile surface (see [16] for an illustration). The generators $l(v)$ of the auxiliary developable surface Φ are the *curvature axes* of the spine curve,

$$l(v) = x(v) + \frac{1}{\kappa(v)}\,\vec{n}(v) + \lambda\,\vec{b}(v), \qquad \lambda \in \mathbb{R}, \tag{8}$$

where κ is again the curvature of the spine curve. In consequence of this kinematical generation, the profile surface has a second order contact with the surface of revolution that is generated by simply rotating the cross–section curve $c(u)$ around the generator $l(v)$. Thus, if the cross–section curve is G^2-continuous, then the profile surface and the corresponding

surface of revolution meet along $l(v)$ with G^2-continuity. Since continuity of the curvature axes (8) corresponds to G^2-continuity of the spine curve $x(v)$, we obtain:

Proposition 6 *A profile surface with G^2-continuous spine and cross–section curves is G^2–continuous, too.*

2.3. Singularities and convexity

We analyze singularities and principal curvatures of profile surfaces. A point of the profile surface $s(u, v)$ is called *singular* iff the first derivatives are linearly dependent. Owing to Proposition 1, this is only possible if $(\partial/\partial v)\, s(u, v) = \vec{0}$. In consequence of its kinematical generation, the profile surface $s(u, v)$ has singular points exactly at intersections of cross–section curve and curvature axis $l(v)$. Thus, we obtain the following condition:

Corollary 7 *A profile surface has no singular points if the condition*

$$c_2(u)\cos\Omega(v) - c_3(u)\sin\Omega(v) < 1/\kappa(v) \tag{9}$$

is satisfied for all u, v.

As a sufficient condition (which may be useful in applications), one may use the inequality $\|c(u)\| < 1/\kappa_{max}$ that is easier to deal with.

In order to analyze the shape of $s(u, v)$ we examine the distribution of the Gaussian curvature $K(u, v) = \kappa_1\,\kappa_2$. Here, the $\kappa_i(u, v)$ are the *principal curvatures* of the profile surface $s(u, v)$. Since the normal vector

$$\vec{N}(u, v) = \frac{\dot c_3 \vec{f}_2 - \dot c_2 \vec{f}_3}{\sqrt{\dot c_2{}^2 + \dot c_3{}^2}} = \frac{(\dot c_3 \sin\Omega - \dot c_2 \cos\Omega)\vec{b} + (\dot c_3 \cos\Omega + \dot c_2 \sin\Omega)\vec{n}}{\sqrt{\dot c_2{}^2 + \dot c_3{}^2}} \tag{10}$$

of the profile surface lies in the normal plane of the spine curve $x(v)$, and owing to Proposition 3, the principal curvature κ_1 is equal to the curvature κ_u of the cross–section curve,

$$\kappa_1 = \kappa_u = \frac{\dot c_2 \ddot c_3 - \ddot c_2 \dot c_3}{(\dot c_2{}^2 + \dot c_3{}^2)^{3/2}}. \tag{11}$$

On the other hand, the principal curvature κ_2 is related to the curvature κ_v of the isoparametric curves $u = \mathrm{const.}$ of the profile surface via *Meusnier's formula*, cf. [18]:

$$\kappa_2 = \kappa_v \cos\theta, \tag{12}$$

where θ is the angle between the normal $\vec{n}(v)$ of the isoparametric curve $u = \mathrm{const.}$ and the normal $\vec{N}(u, v)$ of the surface $s(u, v)$. Note that the normals of the spine curve and of the isoparametric curves $u = \mathrm{const.}$ are identical, as these curves have identical fields of tangent vectors (Proposition 1).

In order characterize the *shape* of profile surfaces, we try to find the curves on $s(u, v)$ that are formed by *parabolic points*, i.e. points with vanishing Gaussian curvature. These curves separate elliptic ($K > 0$, locally convex) and hyperbolic ($K < 0$, hence non–convex) parts of the surface. Resulting from

$$K = \kappa_1\,\kappa_2 = \kappa_u\,\kappa_v\,\cos\theta, \tag{13}$$

there are three possible cases which produce parabolic points:

1. The curvature of the cross–section curve vanishes ($\kappa_u(u) = 0$), Thus, an inflection or flat point of the cross–section curve generates an isoparametric parabolic curve $u = $ constant on the profile surface $\mathsf{s}(u, v)$.

2. The curvature κ_v of an isoparametric curve $u = $ const. vanishes. This is the case, if the curvature $\kappa(v)$ of the spine curve $\mathsf{x}(v)$ vanishes. Thus, an inflection or flat point of the spine curve generates an isoparametric parabolic curve $v = $ constant on the profile surface $\mathsf{s}(u, v)$.

3. The vectors $\vec{\mathsf{N}}(u, v)$ and $\vec{\mathsf{n}}(v)$ are perpendicular, hence $\cos\theta = 0$. Owing to (10), these parabolic curves are characterized by the following implicit equation in the uv–parameter space of the profile surface $\mathsf{s}(u, v)$:

$$\dot{c}_3(u) \cos \Omega(v) + \dot{c}_2(u) \sin \Omega(v) = 0. \tag{14}$$

In computer aided geometric design, conditions that guarantee the convexity of a surface are required in various applications. In the case of general tensor–product B–spline surfaces, such conditions have been derived by several authors, see e.g. [9]. However, these conditions may produce large systems of non–linear inequalities that are difficult to deal with. In particular, this is the case for truly parametric surface representations.

In the case of profile surfaces, however, the convexity can be controlled with the help of the differential geometric properties, as follows.

Proposition 8 *Consider a profile surface patch $\mathsf{s}(u, v)$ with spine curve $\mathsf{x}(v)$ and cross–section curve $\mathsf{c}(u)$. If both the spine curve and the cross–section curve have non–vanishing curvature everywhere, and provided that the normal $\vec{\mathsf{N}}(u, v)$ of the profile surface patch is never parallel to the binormal $\vec{\mathsf{b}}(v)$ of the spine curve, then the surface patch has no parabolic points.*

Consider a convex cross–section curve $\mathsf{c}(u)$. Let δ denote the maximum angle $\angle(\dot{\mathsf{c}}(u_0), \dot{\mathsf{c}}(u_1))$ between the tangent vectors of the convex cross–section curve. Moreover, let Ω_{max} (resp. Ω_{min}) be the maximum (resp. minimum) value of the right–hand side of (6) in the parameter interval $v \in [v_0, v_1] \subset \mathbb{R}$.

Corollary 9 *If $\delta < \pi$ and $\Omega_{max} - \Omega_{min} < \pi - \delta$, then there exists a suitable constant Ω_0 in (6) such that the profile surface patch has positive Gaussian curvature at all points. In addition, the substitution $\Omega_0 \to \Omega_0 + \pi$ leads to a profile surface patch with negative Gaussian curvature. If $\delta \geq \pi$, however, then it is impossible to construct a profile surface patch without parabolic points.*

In the case of locally convex profile surfaces, equation (14) can be used for cutting the patch into convex and non–convex parts. Fig. 2 shows two profile surface patches and their parabolic lines. In the first example (left), the cross–section curve has an inflection point that generates an isoparametric parabolic curve on the profile surface. The other two isoparametric curves result from (14).

In the second case the cross–section curve is convex with $\delta = \pi$. Both cross–section curves are cubic curves. Therefore the implicit equation (14) is quadratic in s and can be parameterized with two square root functions $s_{1,2}(v)$.

Note that Fig. 2 does not show the exact profile surfaces. Instead, we have drawn two rational approximations to them. The approximating surfaces have been generated with the methods that are described below. Both surfaces are rational tensor–product Bézier patches of degree $(9, 3)$.
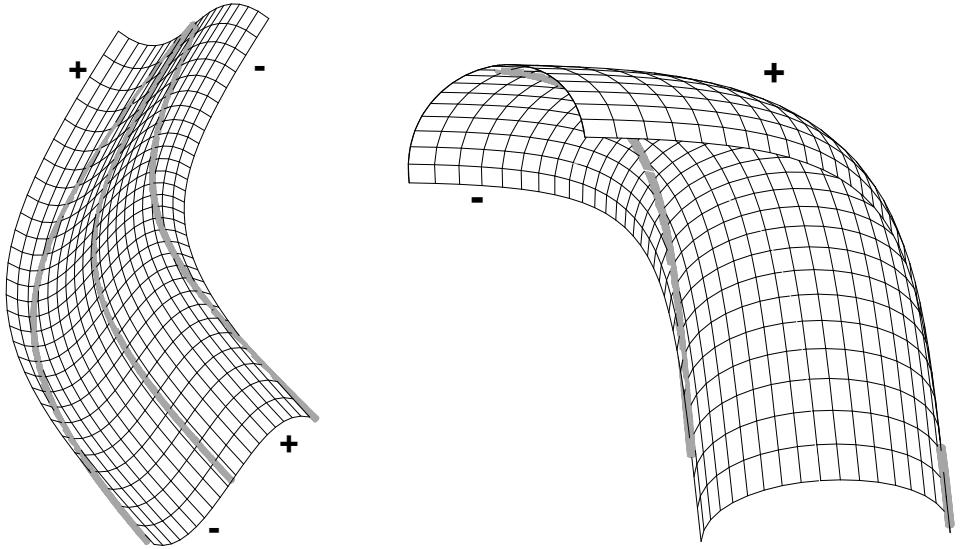
Figure 2: Parabolic lines on profile surfaces and signs of the Gaussian curvatures.

3. Rational approximation of the RMF

Based on spatial Pythagorean hodograph (PH) curves we describe a technique for generating rational approximation of rotation minimizing frames and profile surfaces.

3.1. Spatial PH cubics

A cubic Bézier curve (see [5]) is given by the parametric representation

$$\mathsf{x}(v) = \sum_{i=0}^{3} \mathsf{b}_i \, B_i^3(v), \qquad v \in [0,1] = [v_0, v_1], \tag{15}$$

with control points $\mathsf{b}_i \in \mathbb{R}^3$ and Bernstein polynomials $B_i^n(v) = \binom{n}{i} v^i (1-v)^{n-i}$, cf. [5]. If the components $\dot{x}_j(v)$ of the first derivative vector $\dot{\mathsf{x}}(v)$ (which is sometimes referred to as the *hodograph* of the curve) satisfy the Pythagorean condition

$$\dot{x}_1(v)^2 + \dot{x}_2(v)^2 + \dot{x}_3(v)^2 = p(v)^2 \tag{16}$$

for some real polynomial $p = p(v)$, then this curve is called a *Pythagorean hodograph* (PH) *cubic*, see [3].

Consider the difference vectors $\Delta \mathsf{b}_i = \mathsf{b}_i - \mathsf{b}_{i-1}$ and let $\theta_{i,j}$ be the angle between the vectors $\Delta \mathsf{b}_i$ and $\Delta \mathsf{b}_j$. Moreover, let ψ be the angle between $\Delta \mathsf{b}_1 \times \Delta \mathsf{b}_2$ and $\Delta \mathsf{b}_2 \times \Delta \mathsf{b}_3$. According to a result by Farouki and Sakkalis [3], the Bézier curve (15) is a PH cubic iff the conditions

$$\theta_{1,2} = \theta_{2,3} \quad \text{and} \quad \cos \psi = \frac{2\,L_2^2}{L_1 L_3} - 1 \tag{17}$$

with $L_i = \|\Delta \mathsf{b}_i\|$ are satisfied. The parametric speed $\sigma(v) = \|\dot{\mathsf{x}}(v)\|$, the curvature and torsion

of PH cubics are given by the expressions

$$\sigma(v) = 3 \left(L_1 \, B_0^2(v) + L_2 \, \cos\theta \, B_1^2(v) + L_3 \, B_2^2(v) \right),$$

$$\kappa(v) = \frac{6 \, L_2 \, |\sin\theta_{1,2}|}{\sigma(v)^2}, \qquad \tau(v) = \frac{-3 \, L_1 \, L_3 \, \sin\psi}{L_2 \, \sigma(v)^2}. \tag{18}$$

The ratio κ/τ is constant, hence any PH cubic is a *curve of constant slope* (also called a *cubic helix*). A thorough geometrical discussion of cubic and quartic curves with constant slope has been given by Wunderlich [21].

The Frenet–Serret frame of a PH cubic is formed by the unit tangent $\vec{t}(v) = \dot{\mathsf{x}}(v)/\sigma(v)$, along with the normal and binormal vectors

$$\vec{n}(v) = \frac{\sigma(v) \, \ddot{\mathsf{x}}(v) - \dot{\sigma}(v) \, \dot{\mathsf{x}}(v)}{6 \, L_2 \, |\sin\theta_{1,2}| \, \sigma(v)}, \qquad \vec{b}(v) = \frac{\dot{\mathsf{x}}(v) \times \ddot{\mathsf{x}}(v)}{6 \, L_2 \, |\sin\theta_{1,2}| \, \sigma(v)}. \tag{19}$$

Clearly, the three vectors are quadratic rational functions of the curve parameter v; they describe three circles on the unit sphere. Thus, the spherical part of the motion of the Frenet–Serret frame (which is governed by the special orthogonal matrix $A(v) = \{\vec{t}(v), \vec{n}(v), \vec{b}(v)\}$) is simply a *rotation* with a certain constant axis, but with varying angular velocity.

PH cubics are one of the simplest representatives of curves with rational Frenet–Serret motion, the so–called *RF–curves*. These curves have been studied recently by Wagner and Ravani [19].

The approximation scheme which is described below is based on the following advantageous features of PH cubics:

1. *PH cubics are equipped with rational frames.* This fact is true for any spatial PH curve, see [6]. In the cubic case, even the Frenet–Serret frame is rational.

2. *The integral (6) can be evaluated analytically without numerical integration.* This fact will facilitate the rational approximation of the RMF, see Section 3.3.

3. *An arbitrary space curve can be approximated by a cubic G^1 PH spline curve with any desired accuracy*, see Section 3.2.

With the help of the third property, the RMF approximation can be applied to any spatial spine curves. In a first step, the spine curve is approximately converted into a cubic PH spline curve. Then, the RMF of the individual PH cubics is approximated as described below.

3.2. G^1 Hermite interpolation

We summarize some results on G^1 Hermite interpolation with PH cubics. More details can be found in [8] and the recent Master thesis [1].

As observed by Wagner and Ravani [19], PH cubics are capable of matching G^1 Hermite boundary data, i.e. boundary points p_0, p_1 with associated unit tangents $\vec{t}_0$, $\vec{t}_1$. For the convenience of the reader, an algorithm for computing the solutions (which is equivalent to the results in [19]) is provided in Table 1. This algorithm is based on the geometric characterization (17) of the control polygon of PH cubics. It computes the Bézier points b_i and b_2 of the interpolating PH cubic.

Note that the quadratic equation (∗) does not always have real solutions. Also, even if real solutions $X_{1/2}$ exist, it may happen that the interpolating PH cubic matches the directions of the unit tangents $\vec{t}_0$, $\vec{t}_1$ but has the opposite orientation. Finally, if real solutions with the

INPUT: Boundary points $p_0 = b_0$, $p_1 = b_3$ with associated unit tangents $\vec{t}_0$, $\vec{t}_1$.

1. $m_1 = (\vec{t}_0 \cdot \vec{t}_1)\vec{t}_1 - \vec{t}_0$, $m_2 = \vec{t}_1 - (\vec{t}_0 \cdot \vec{t}_1)\vec{t}_0$.

2. $\lambda_1 = \dfrac{m_1 \cdot (b_3 - b_0)}{m_1 \cdot t_0}$, $\lambda_2 = \dfrac{m_2 \cdot (b_0 - b_3)}{m_2 \cdot t_1}$.

3. $n_1 = b_0 + \lambda_1 \vec{t}_0$, $n_2 = b_3 + \lambda_2 \vec{t}_1$.

4. Solve the quadratic equation

$$(|\lambda_1| - X)(|\lambda_2| - X) - 2X^2(1 + \vec{t}_0 \cdot \vec{t}_1) = \frac{2\|n_1 - n_2\|^2}{1 - \vec{t}_0 \cdot \vec{t}_1} \qquad (*)$$

for the unknown X.

OUTPUT: Inner Bézier points (2 solutions) $b_1 = n_1 - X_{1/2}\vec{t}_0$, $b_2 = n_2 + X_{1/2}\vec{t}_1$.

Table 1: G^1 Hermite interpolation with PH cubics.

correct orientation at the boundaries exist, then one will get two different solutions in general, corresponding to the possibly different roots of $(*)$. One should then pick the solution with the shorter control polygon.

Theorem 10 *Consider a spatial curve* $p(s)$, $s \in I \subset \mathbb{R}$, *which is assumed to be* C^5 *in a neighbourhood of* $p(0)$. *Without loss of generality, the parameter* s *is chosen as the arc length of the curve, hence* $\|\dot{p}(s)\| \equiv 1$. *In addition, as a technical assumption, the curve has non–zero curvature* $\kappa(0)$ *at* $p(0)$.

Consider the curve segment $s \in [0, h]$ *for some positive stepsize* h. *This curve segment provides the following* G^1 *Hermite boundary data:*

$$p_0 = p(0), \quad \vec{t}_0 = \dot{p}(0), \quad p_1 = p(h), \quad and \quad \vec{t}_1 = \dot{p}(h). \qquad (20)$$

In order to find an interpolating Pythagorean hodograph cubic we apply the G^1 *Hermite interpolation procedure (see Table 1) to these data.*

(i) *If the stepsize* h *is sufficiently small, then the interpolation problem has two real solutions. One of these solutions matches the shape of the original curve.*

(ii) *The PH cubic which matches the original shape has approximation order four. More precisely, there exists a reparameterization* $v = v(t)$ *satisfying* $v(0) = 0$ *and* $v(1) = 1$, *such that*

$$\max_{t \in [0,1]} \|x(v(t)) - p(h\,t)\| = O(h^4). \qquad (21)$$

Proof: The proof is based on the canonical Taylor expansion

$$p(s) = \begin{pmatrix} s - \frac{1}{6}\kappa_0{}^2 s^3 - \frac{1}{8}\kappa_0\kappa_1 s^4 + \dots \\ \frac{1}{2}\kappa_0 s^2 + \frac{1}{6}\kappa_1 s^3 + (\frac{1}{24}\kappa_2 - \frac{1}{24}\kappa_0{}^3 - \frac{1}{24}\kappa_0\tau_0{}^2)s^4 + \dots \\ \frac{1}{6}\kappa_0\tau_0 s^3 + (\frac{1}{12}\kappa_1\tau_0 + \frac{1}{24}\kappa_0\tau_1)s^4 + \dots \end{pmatrix} \qquad (22)$$

of a space curve with respect to its arc–length parameter. This expansion is an immediate consequence of the Frenet–Serret formulas, see [18]. The coefficients κ_i resp. τ_i are the values of the derivatives of curvature and torsion with respect to the arc length at $p(0)$. With the
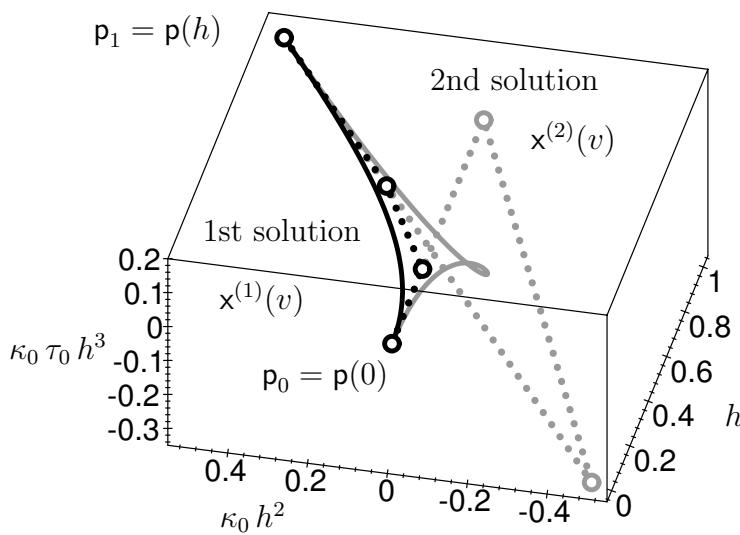
Figure 3: Asymptotic shape of the interpolating PH cubics for stepsize $h \to 0$.

help of this expansion we generate Taylor expansions of the G^1 Hermite boundary data (20),

$$\mathbf{p}_0 = \begin{pmatrix} 0 \\ 0 \\ 0 \end{pmatrix}, \quad \vec{t}_0 = \begin{pmatrix} 1 \\ 0 \\ 0 \end{pmatrix}, \quad \mathbf{p}_1 = \begin{pmatrix} h + \ldots \\ \frac{1}{2} \kappa_0 h^2 + \ldots \\ \frac{1}{6} \kappa_0 \tau_0 h^3 + \ldots \end{pmatrix}, \quad \vec{t}_1 = \begin{pmatrix} 1 - \frac{1}{2} \kappa_0^2 h^2 + \ldots \\ \kappa_0 h + \frac{1}{2} \kappa_1 h^2 + \ldots \\ \frac{1}{2} \kappa_0 \tau_0 h^2 + \ldots \end{pmatrix}. \quad (23)$$

Due to space limitations, only the leading terms of the expansions are shown. The Hermite interpolation procedure (see Table 1) is applied to these expansions, leading to Taylor expansions for all occurring variables. This is most efficiently done with the help of computer algebra tools such as Maple or Mathematica. In step 4 of the procedure, one has to generate the quadratic equation $(*)$, leading to

$$-3 X^2 - X h + (X^2 \kappa_0^2 + \frac{1}{4}) h^2 + (X^2 \kappa_0 \kappa_1 - \frac{1}{12} X \kappa_0^2) h^3 + \ldots = \frac{1}{36} \tau_0^2 h^4 + \ldots. \quad (24)$$

The discriminant of this equation has the Taylor expansion

$$\frac{1}{9} h^2 + \left(\frac{6 \kappa_0^4 - \kappa_1^2 - 4 \kappa_0^2 \tau_0^2}{432 \kappa_0^2} + \frac{11 \kappa_0^2}{216} \right) h^4 + \ldots, \quad (25)$$

hence two real solutions exist, provided that the stepsize h is sufficiently small. (The technical assumption $\kappa_0 \neq 0$ is needed for generating this expansion, as higher order terms of (24) with denominator κ_0 come into play.) Thus, we obtain two solutions $\mathbf{x}^{(j)}$. After computing the control points we obtain from (15) the expansions

$$\mathbf{x}^{(1)}(v) = \begin{pmatrix} v h + \ldots \\ \frac{1}{2} v^2 \kappa_0 h^2 + \ldots \\ \frac{1}{6} v^3 \kappa_0 \tau_0 h^3 + \ldots \end{pmatrix} \quad \text{and} \quad \mathbf{x}^{(2)}(v) = \begin{pmatrix} (3 v - 6 v^2 + 4 v^3) h + \ldots \\ -\frac{3}{2} v^2 + 2 v^3 \kappa_0 h^2 + \ldots \\ (-v^2 + \frac{7}{6} v^3) \kappa_0 \tau_0 h^3 + \ldots \end{pmatrix}. \quad (26)$$

The spatial curves that are generated by the leading terms of these expansions, along with their control polygons (dotted), are shown on Fig. 3. Note that the units of the coordinate axes are h, $\kappa_0 h^2$, and $\kappa_0 \tau_0 h^3$. If the stepsize h gets smaller, the shape of the solutions becomes more and more similar to the curves shown in the figure. By comparing the expansions (26)

and (22) it can clearly be seen that the first solution matches the shape of the original curve. This proves the first part of the Theorem.

In order to prove (ii), we have to find a suitable reparameterization. Applying the substitution

$$
\begin{aligned}
v(t) \;=\; & t + \frac{t(t-1)\kappa_1}{4\,\kappa_0}\,h \\
& + \frac{t(t-1)(10\,t\,\kappa_1{}^2 - 8\,t\,\kappa_0{}^4 - 8\,t\,\kappa_0{}^2\tau_0{}^2 + 4\,\kappa_0{}^2\tau_0{}^2 + 12\,\kappa_0\kappa_2 - 17\,\kappa_1{}^2 + 4\,\kappa_0{}^4)}{96\,\kappa_0{}^2}\,h^2
\end{aligned}
\tag{27}
$$

one gets $\mathsf{x}^{(1)}(v(t)) - \mathsf{p}(h\,t) = O(h^4)$. Here, higher order terms of both $\mathsf{x}^{(1)}(v)$ and $\mathsf{p}(s)$ (not shown) are taken into account. This completes the proof. $\qquad\square$

With the help of a somewhat different approach, the first part (i) of the Theorem has been proved in [8]. That article also addresses the case of inflections or flat points ($\kappa(0) = 0$). As conjectured there (and shown for points with $\kappa_1 = \dot\kappa(0) \neq 0$), the first assertion (i) is also true in this case. The second part (ii) of the Theorem is due to the recent Master thesis of Eriksson [1].

In consequence of these observations, any space curve (which is assumed to consist of C^5 segments) can approximately be converted into a cubic G^1 PH spline curve with any desired accuracy. The PH spline curve is found by sampling sufficiently many G^1 Hermite data from the curve and filling in PH cubics.

3.3. Rational frames of PH cubics

In order to generate rational frames of PH curves we use again the characterization (17) of PH cubics. Starting with the rational Frenet–Serret frame (19), other rational frames can easily be constructed by applying an additional rotation around the tangent vector $\vec{\mathsf{t}}$. Let $\widehat{\mathsf{n}}$ and $\widehat{\mathsf{b}}$ be the numerators of $\vec{\mathsf{n}}$ and $\vec{\mathsf{b}}$ in (19), respectively. Resulting from the standard rational parameterization of the unit circle,

$$
(\sin\varphi,\,\cos\varphi) = \left(\frac{2w}{(1+w^2)},\, \frac{(1-w^2)}{(1+w^2)} \right) \quad \text{with} \quad w = \tan(\varphi/2),
\tag{28}
$$

we may choose the following basis vectors $\vec{\mathsf{f}}_2(v)$, $\vec{\mathsf{f}}_3(v)$ of the frame,

$$
\vec{\mathsf{f}}_2 = \frac{2w\,\widehat{\mathsf{b}} + (1-w^2)\,\widehat{\mathsf{n}}}{(1+w^2)\,6L_2|\sin\theta|\,\sigma}, \qquad \vec{\mathsf{f}}_3 = \frac{(1-w^2)\,\widehat{\mathsf{b}} - 2w\,\widehat{\mathsf{n}}}{(1+w^2)\,6L_2|\sin\theta|\,\sigma},
\tag{29}
$$

where $\sigma = \sigma(v)$ has been introduced in (18). By choosing a rational function $w = w(v)$ of degree n/n we obtain from (29) a rational frame of degree $2(n+1)$.

In order to obtain a rotation minimizing frame from (29), the solution of (6) has to be substituted in $w(v) = \tan(\frac{1}{2}\Omega(v))$. Owing to (18), the integral (6) can be evaluated analytically,

$$
\begin{aligned}
\Omega(v) - \Omega_0 \;=\; & -\int_0^v \tau(t)\,\|\dot{\mathsf{x}}(t)\|\,dt = \frac{3L_1 L_3 \sin\psi}{L_2} \int_0^v \frac{dt}{\sigma(t)} \\
\;=\; & \frac{2}{a}\,\mathrm{sgn}(\sin\psi)\,\sqrt{L_1 L_3 - L_2^2}\,\arctan\!\left(\frac{c\,v - b}{a}\right)
\end{aligned}
\tag{30}
$$

where

$$a = \sqrt{L_1 L_3 - L_2^2 \cos^2 \theta}, \quad b = L_1 - L_2 \cos \theta, \quad \text{and} \quad c = L_1 - 2L_2 \cos \theta + L_3, \qquad (31)$$

with a suitably chosen integration constant Ω_0. The argument of the square root is positive, as (17) implies $L_1 L_3 \geq L_2^2$. The function $\Omega(u)$ is monotonic and has exactly one inflection point at $t = b/c$. For the *total rotation* $\Delta\Omega$ of Ω (for v varying in $(-\infty, +\infty) = \mathbb{R}$) we obtain

$$\Delta\Omega = \lim_{t \to \infty} \Omega - \lim_{t \to -\infty} \Omega < 2\pi. \qquad (32)$$

In order to obtain from (29) a rational representation of the rotation minimizing frame, we need to find a rational expression for

$$w(v) = \tan(\frac{1}{2}\Omega(v)) = \tan\left(\frac{\Omega_0}{2} + \underbrace{\frac{1}{a} \operatorname{sgn}(\sin \psi) \sqrt{L_1 L_3 - L_2^2} \arctan\left(\frac{cv - b}{a}\right)}_{= k} \right). \qquad (33)$$

Clearly, such a rational expression would exist if k were a non–negative integer. In our application, however, we have $0 < k \leq 1$. Moreover, the case $k = 1$ corresponds to the case $\theta = 0$ where the PH cubic degenerates into a straight line. In the next section we describe a numerical procedure that leads to a rational approximation $W(v)$ of (33).

As mentioned in [20], generating the rotation–minimizing frame from the Frenet–Serret frame along with equation (6) may entail numerical problems at points with almost vanishing torsion. In our situation, such problems do not appear; owing to the geometric characterization of $\vec{n}(v)$ and $\vec{b}(v)$ as circles, the Frenet–Serret frame can be computed in a robust way. The computation of $\Omega(v)$ is numerically stable also, as no numerical quadrature is required. Note that the function $|\tau(v)|$ has no local minimum in $[v_0, v_1] = [0, 1]$.

3.4. Approximation of the RMF

Next we turn our attention to the approximation of the function $w(v)$, $v \in [0, 1]$ with a rational function of degree n/n. Consider the C^1 Hermite boundary data of $w(v)$,

$$w_0 = w(0), \quad w_1 = w(1), \quad s_0 = \dot{w}(0), \text{ and } s_1 = \dot{w}(1). \qquad (34)$$

The rational approximation is to interpolate these data, since we wish to represent both the rotation minimizing frame and its derivatives exactly at the segment boundaries. Consequently, if two spine curves (PH cubics) meet with G^1-continuity, the interpolation of the Hermite data (34) guarantees G^1-continuity of the rational approximation to the rotation minimizing frame, too (cf. Proposition 5).

The function $w(v)$ is strictly monotonic, see (33). Here we consider the case $\dot{w}(v) > 0$; the remaining case ($\dot{w}(v) < 0$) can be discussed analogously. Thus, we may assume that

$$w_0 < w_1, \quad s_0 > 0 \quad \text{and} \quad s_1 > 0. \qquad (35)$$

The rational approximation $W(v)$ shall have the form

$$W(v) = \frac{\gamma_0(1 - v)^2 + \gamma_1 2(1 - v)v + \gamma_2 v^2}{\beta_0(1 - v)^2 + \beta_1 2(1 - v)v + \beta_2 v^2} \qquad (36)$$
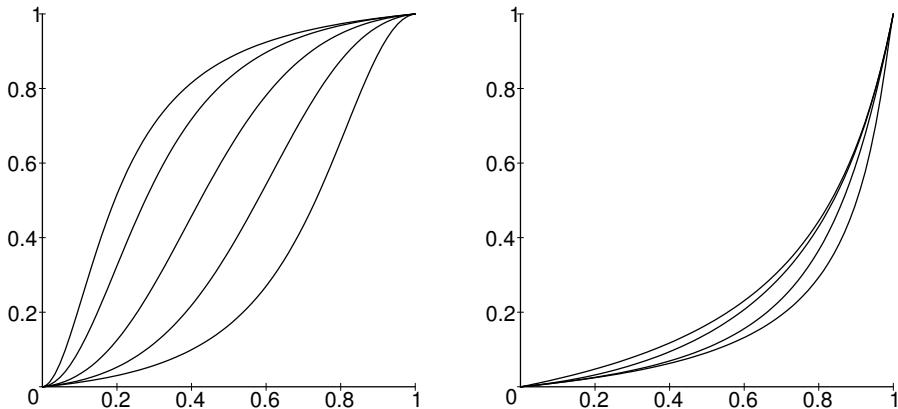
Figure 4: Biquadratic rational Hermite interpolation functions $W(v)$.

with the coefficients

$$\gamma_0 = w_0\beta_0, \quad \gamma_1 = s_1(w_0(\lambda+2)+s_0)/2, \quad \gamma_2 = w_1\beta_2 \quad \text{and}$$
$$\beta_0 = s_1, \quad \beta_1 = s_1(\lambda+2)/2, \quad \beta_2 = (w_1-w_0)(\lambda+2)-s_0 \tag{37}$$

that depend on one free parameter λ. We obtain a one–parametric family of functions that interpolate the boundary data w_0, w_1 with associated derivatives s_0, s_1. As an example, Fig. 4 shows two families of such Hermite interpolation functions for different boundary data.

Lemma 11 *If the boundary data fulfil the monotonicity condition (35) and if the design parameter λ satisfies the inequality*

$$\lambda > \lambda^* = \frac{s_0}{w_1 - w_0} - 2, \tag{38}$$

then the rational Hermite interpolant $W(v)$, $v \in [0,1]$, is monotonic and has no poles.

Proof: Combining (35) and (38), the weights β_0, β_1, β_2 of $W(v)$ can be shown to be non–negative, hence $W(v)$ has no poles within $[0,1]$. In order to prove monotonicity we have to examine the numerator of the first derivative $\dot{W}(v)$. Using its Bernstein–Bézier representation we obtain

$$s_0\, s_1^2\, (1-v)^2 + s_1\,(w_1-w_0)\,\beta_2\, 2(1-v)v + s_1\,\beta_2{}^2\, v^2. \tag{39}$$

Owing to (35) and (38), all coefficients can be shown to be positive, hence the first derivative has no roots within $[0,1]$. $\qquad\square$

In order to obtain the best available representation of the rotation minimizing frame, a good approximation of the derivative $\dot{\Omega}$ is necessary. That is, we try to approximate the *velocity distribution* of the rotation minimizing frame. We find the optimum value of λ by minimizing the objective function

$$I(\lambda) = \int_0^1 \left(\frac{d}{dv}\left[2\arctan(W_\lambda(v))\right] - \dot{\Omega}(v)\right)^2 dv = \int_0^1 \underbrace{\left(\frac{2\dot{W}_\lambda(v)}{1+W_\lambda^2(v)} - \dot{\Omega}(v)\right)^2}_{=\,F_\lambda(v)} dv. \tag{40}$$
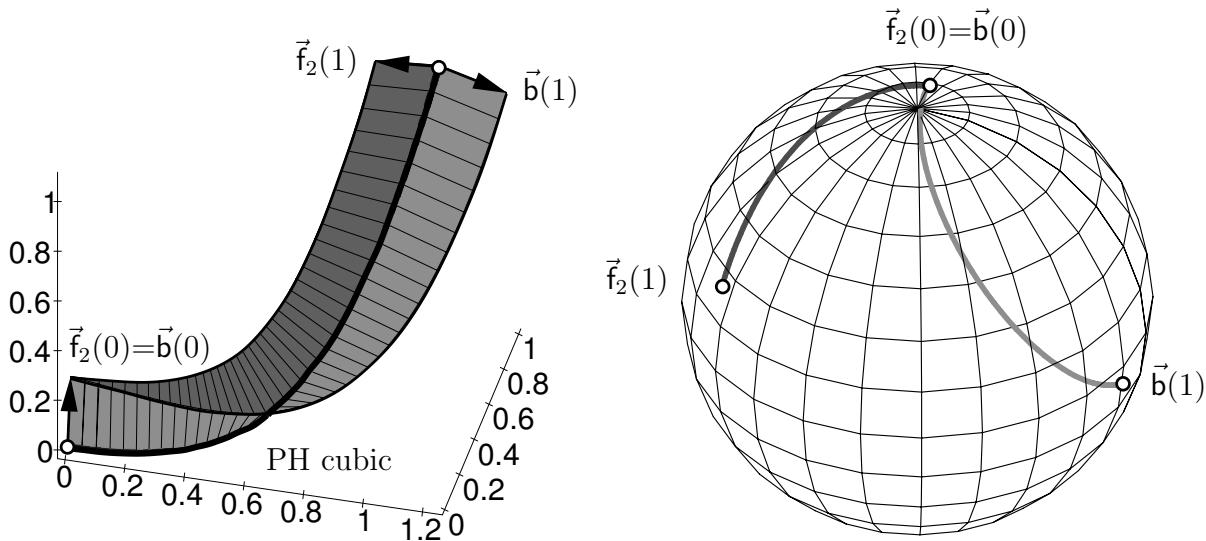
Figure 5: Rotation minimizing frame vs. Frenet-Serret frame of a PH cubic. The vector fields $\vec{f}_2(v)$ and $\vec{b}(v)$ along with the PH cubic (left), and the associated spherical indicatrices $\vec{f}_2(v)$ and $\vec{b}(v)$ (right)

Note that $F_\lambda(v)$ is a rational function of degree $8/8$ in v, hence the exact value of the integral could be found via partial fraction decomposition. For the practical implementation, however, it is sufficient to use a standard numerical quadrature formula

$$I(\lambda) \approx \widehat{I}(\lambda) = \sum_{j=0}^{k} \alpha_j F_\lambda(u_j) \tag{41}$$

such as Simpson's rule. A suitable initial guess for the Newton algorithm is $\lambda^* + \epsilon$, cf. Lemma 11.

An example is shown in Fig. 5. The PH cubic is shown in the left figure, along with the binormal vectors $\vec{b}(v)$ and the basis vector $\vec{f}_2(v)$ of the rational approximation to the rotation minimizing frame (chosen such that $\vec{f}_2(0) = \vec{b}(0)$). In addition, the corresponding spherical curves have been drawn (right figure). Note that the spherical indicatrix $\vec{f}_2(v)$ is much shorter than the corresponding curve generated by the binormal $\vec{b}(v)$.

In this example, the objective function (40) is shown in Fig. 6 (right). The minimum $\lambda_{min} = -0.3055$ was found with a standard Newton algorithm, corresponding to $\widehat{I}(\lambda_{min}) = 0.000233$. The function $\dot{\Omega}(v)$ and its rational approximation (left figure) are virtually indistinguishable.

According to our numerical experiments, the accuracy of the rational approximation to the RMF will be sufficient in most applications. If necessary, it can be improved by increasing the number of segments that is used for constructing the cubic PH spline curve.

3.5. Profile surface approximation

As the final step, the results of the previous sections are gathered in order to generate rational approximations of profile surfaces. From a given PH space cubic $x(v)$ as spine curve, along with the planar rational curve $c(u) = (0, c_2(u), c_3(u))^\top$ as cross–section curve, we obtain the
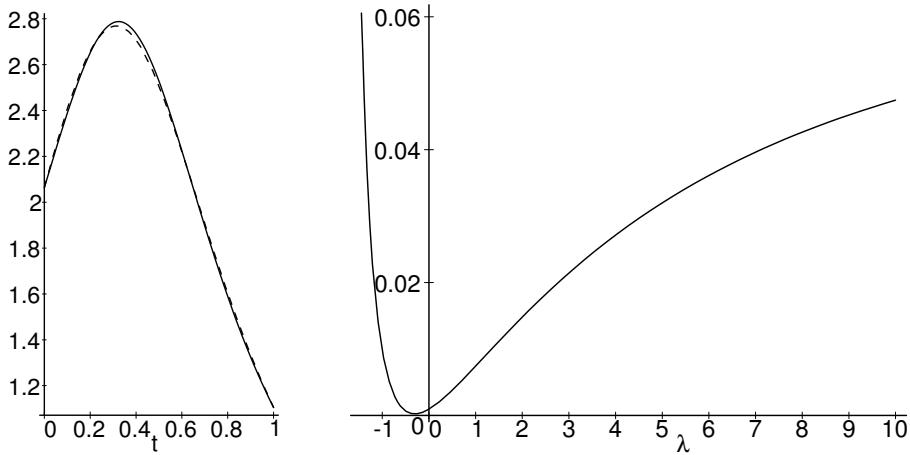
Figure 6: The function $\dot{\Omega}(v)$ and its rational approximation (left); objective function $\widehat{I}(\lambda)$ (right).

rational sweeping surface

$$\mathsf{s}(u, v) = \mathsf{x} + \frac{c_2 \left[2\, W\, \widehat{\mathsf{b}} + (1 - W^2)\, \widehat{\mathsf{n}}\right] + c_3 \left[(1 - W^2)\, \widehat{\mathsf{b}} + 2W\, \widehat{\mathsf{n}}\right]}{(1 + W^2)\, 6\, L_2\, |\sin\theta|\, \sigma}, \tag{42}$$

where the quantities $W(v)$, $\widehat{\mathsf{b}}(v)$, $\widehat{\mathsf{n}}(v)$, and $\sigma(v)$ have been introduced earlier. This sweeping surface is a rational approximation to the profile surface. Let n denote the degree of $W(v)$ and m the degree of $\mathsf{c}(u)$. The profile surface approximation $\mathsf{s}(u, v)$ has the degree $(2n+5, m)$.

The quality of the rational approximation to the profile surface may be checked in various ways. Firstly, one can use the value $\widehat{I}(\lambda_{min})$ of the objective function. As another criterion, one may check whether the properties of Section 2 are (approximately) satisfied. For instance, a necessary condition for the curvature line property 3 is orthogonality of the parameter lines, i.e.,

$$O(u, v) = \frac{\left(\frac{\partial}{\partial u}\mathsf{s}(u, v), \frac{\partial}{\partial t}\mathsf{s}(u, v)\right)}{\left\|\frac{\partial}{\partial u}\mathsf{s}(u, v)\right\| \left\|\frac{\partial}{\partial t}\mathsf{s}(u, v)\right\|} = 0. \tag{43}$$

The quantity $O(u, v)$ measures the cosine of the angle between the parameter lines at the point $\mathsf{s}(u, v)$. For the profile surface approximation shown in Fig. 1, $|O(u, v)| < 3.2\ 10^{-7}$ is satisfied at all $u, v \in [0, 1]$. Hence, the a parameter lines are very close to forming an orthogonal net. By contrast, in the case of the sweeping surface which is generated with the Frenet–Serret frame, the upper bound is 0.08.

If the cross–section curve is degenerated into a straight line, the profile surface should be a developable surface. Consequently, the Gaussian curvature K can be used as an accuracy criterion. Fig. 7 shows two ruled surfaces, generated by the rational approximation to the RMF (left) and by the Frenet–Serret frame (right).

The Gaussian curvature of the left surface is in the order of the numerical noise ($|K| < 5.0\ 10^{-6}$), thus the surface is 'almost' developable. The Gaussian curvature of the right surface, by contrast, varies between -1.2 and -0.2.
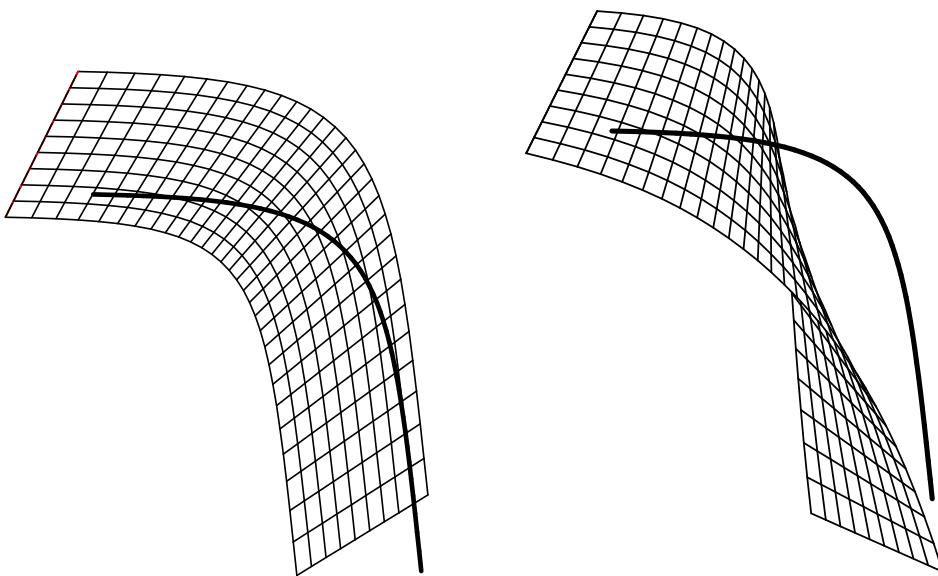
Figure 7: Ruled surfaces, generated by the rational approximation to the rotation minimizing frame (left) and by the Frenet–Serret frame (right).

References

[1] M. ERIKSSON, *Hermite interpolation with spatial Pythagorean hodograph curves.* Master thesis, TU Darmstadt / KTH Stockholm 1999.

[2] G. FARIN, *Curves and surfaces for computer aided geometric design.* 3rd ed., Academic Press, Orlando FL 1992.

[3] R.T. FAROUKI, T. SAKKALIS, *Pythagorean-hodograph space curves.* Adv. Comput. Math. **2**, 41–66 (1994).

[4] H.W. GUGGENHEIMER, *Computing frames along a trajectory.* Comput. Aided Geom. Design **6**, 77–78 (1989).

[5] J. HOSCHEK, D. LASSER, *Fundamentals of Computer Aided Geometric Design.* AK Peters, Wellesley Mass. 1993.

[6] B. JÜTTLER, *Generating Rational Frames of Space curves via Hermite Interpolation with Pythagorean Hodograph Cubic Splines.* In: *Differential/Topological Techniques in Geometric Modeling and Processing'98*, eds. D.P. Choi, H.I. Choi, M.S. Kim and R.R. Martin, Bookplus press, Seoul, South Korea, 1998, pp. 83–106.

[7] B. JÜTTLER, *Rotation Minimizing Spherical Motions.* In: *Advances in Robot Kinematics: Analysis and Control*, eds. J. Lenarčič and M. Husty, Kluwer, Dordrecht 1998, pp. 413–422.

[8] B. JÜTTLER, C. MÄURER, *Cubic Pythagorean Hodograph Spline Curves and Applications to Sweep Surface Modeling.* Comput.–Aided Design **31**, 73–83 (1999).

[9] P.D. KAKLIS, G.D. KORAS, *A Quadratic–Programming Method for Removing Shape–Failures from Tensor–Product B-Spline Surfaces.* Computing [Suppl] **13**, 177–188 (1998).

[10] M.-S. KIM, E.-J. PARK, H.-Y. LEE, *Modelling and animation of generalized cylinders with variable offset space curves.* The Journal of Visualization and Computer Animation **5**, 189–207 (1994).

[11] F. KLOK, *Two moving coordinate frames for sweeping along a 3D trajectory.* Comput. Aided Geom. Design **3**, 217–229 (1986).

[12] E. KREYSZIG, *Differential geometry,* Oxford University Press, London 1964.

[13] R.R. MARTIN, *Principal Patches for Computational Geometry*, Ph.D. thesis, Cambridge University Engineering Department, 1982.

[14] D.S. MEEK, D.J. WALTON, *Geometric Hermite interpolation with Tschirnhausen cubics.* J. Comput. Appl. Math. **81**, 299–309 (1997).

[15] H. POTTMANN, M. WAGNER, *Principal Surfaces.* In: *The Mathematics of Surfaces VII*, eds. T.N.T. Goodman and R.R. Martin, Information Geometers, Winchester 1997, pp. 337–362.

[16] H. POTTMANN, M. WAGNER, *Contributions to Motion Based Surface Design.* Int. J. of Shape Modeling **4**, 183–196 (1998).

[17] K. STRUBECKER, *Differentialgeometrie I–III.* 2nd ed., de Gruyter (Sammlung Göschen), Berlin 1964–1969.

[18] D.J. STRUIK, *Lectures on classical differential geometry.* 2nd ed., Addison–Wesley, Reading (Mass.) 1961.

[19] M. WAGNER, B. RAVANI, *Curves with Rational Frenet–Serret motion.* Comput. Aided Geom. Design **15**, 79–101 (1997).

[20] W. WANG, B. JOE, *Robust computation of the rotation minimizing frame for sweep surface modeling.* Comput.–Aided Design **29**, 379–391 (1997).

[21] W. WUNDERLICH, *Algebraische Böschungslinien dritter und vierter Ordnung.* Sitzungsber., Abt. II, österr. Akad. Wiss., Math.-Naturw. Kl. **181**, 353–376 (1973).